Effect of Dopant Nature on Structures and Lattice Dynamics of Proton conducting BaZrO3

Sahraoui Djamila Zeudmi, Tzonka Mineva

Effect of Dopant Nature on Structures and Lattice Dynamics of Proton-conducting $BaZrO_3$.

D. Zeudmi Sahraoui and T. Mineva*

UMR 5253 CNRS/ENSCM/UM2/UM1, Institut Charles Gerhardt Montpellier, 8 rue de l'Ecole Normale, 34296 Montpellier cedex 5, France

*Corresponding author: tzonka.mineva@enscm.fr,

tel: +33 4 67 16 34 68, fax: +33 4 67 16 34 70

ABSTRACT

The influence of the acceptor-dopants on the local and long range structures and lattice vibrations of barium zirconate has been studied with Density Functional Theory (DFT) based periodic approach. Structural details of $BaZr_{1-x}M_xH_xO_3$ (M = In and Sc, and x = 0.125, 0.25 and 0.375) with protonic defects in three different oxygen configurations are presented and discussed in relation with the results for Y-doped barium zirconates, obtained previously with the same methodology. The oxide symmetry and the short and long range structural arrangements in the M-rich and Zr-rich regions were established nearly independent on the dopant chemical nature, concentration and arrangement in the cell. The O-H bond formation is however strongly influenced by the dopant nature, which is associated with the differences in dopant-oxygen bond character. The computed lattice vibrations in zirconates with Y, In and Sc dopants showed that the O-H vibrations vary by 250 – 1500 cm^{-1} depending on the acceptor-dopant.

Key words: doped $BaZrO_3$, protonic defects, structural properties, lattice vibrations, quantum chemical DFT calculations

1. Introduction

The trivalent cation-doped barium zirconates, $BaZr_{1-x}M_xO_{3-\delta}$, exhibit relatively high proton conductivity while retaining their good mechanical and chemical stability [1]. This property is in the basis of the potential application of doped barium zirconates as proton conducting electrolytes in the fuel cells. Because the chemical nature of doping cations (M^{3+}) can affect the proton transfer processes by order of magnitude [1], recent research works focused on examining how exactly the local and long range structural features of the host oxide vary with M^{3+} and their relation to the proton conductivity. Several characteristics of dopant ions have been proposed to play an important role. These are the ionic radius of the dopant relative to the ionic radius of Zr^{4+} [1-3], the type of M−O bonding in the host oxide, determined by the dopant electronic structure [2,4], Pearson absolute hardness of Zr^{4+} related to that of M^{3+} [5].

At 1600 ˚C, a high solubility of dopant ions into barium zirconate was established for dopants with an ion size, close to that of Zr^{4+} [3]. This high solubility was not strictly related to the same microstructure development and proton conductivity. For instance, In^{3+}, Yb^{3+}, Tm^{3+}, Er^{3+} and Ho^{3+} are characterised as highly soluble at Zr^{4+} site, but at variance In^{3+} led to well-grown grains and lower proton conductivity comparable to that of Sc^{3+}, whereas the other cations were pointed out to exhibit a conductivity close to that of the Y^{3+} doped system [3]. Differences between electronegativities of A and B cations in ABO_3-perovskites were empirically established to correlate with the standard enthalpy and entropy of hydration [6]. More recent results, obtained with Extended X-Ray Absorption Fine Structure (EXAFS) and Raman spectroscopy, for a series of doped barium cerates and zirconates, evidenced that the unique behaviour of the investigated dopants (Y^{3+}, In^{3+} and Gd^{3+}) depends mainly on its electronic structure [4]. It was demonstrated by means of Infra Red (IR) and Raman spectroscopy [7, 8], and X-ray absorption spectroscopy [9] that the highly distorted oxide structures are those showing lower H-transfer capabilities. The local structural disorder in In-$BaZrO_3$ was found uncorrelated with oxygen defects, whereas the Zr^{4+}/In^{3+} charge difference, spread throughout the host oxide, was evidenced as the main driving force of the local distortion [8]. Other studies [4,10,11] where more precise interatomic distance and angle values were derived from the EXAF spectra for barium cerate and barium zirconate doped with In^{3+}, Ga^{3+}, Gd^{3+}, Y^{3+} and Sc^{3+}, concluded that Y^{3+} and Gd^{3+} produced the highest local disorder, which seemed to be the reason for the higher bulk conductivity, compared to that in the zirconates doped with Sc^{3+} and In^{3+}.

Among the various considered M^{3+} cations, Y-doped barium zirconates are the mostly investigated ones, due to their high proton mobility for Y content ≤ 20 % with both experimental [12-22] and theoretical methods [23-29]. Structural, spectroscopic and thermodynamic properties of $In3^{+}$ or Sc^{3+} doped $BaZrO_3$ have been also studied as prototype cases of barium zirconate oxides with the lowest proton conductivity [5, 7, 8, 30-36].

We have thus found it of interest to study systematically the hydrogen insertion into In and Sc doped barium zirconates, considering H-binding to oxygen ions in different local environments (Zr−OH−M, Zr−OH−Zr and M−OH−M). Comparing these findings with our recent results, obtained with same theoretical and numerical details, for Y-doped $BaZrO_3$ with 12.5, 25 and 37.5% of Y content [29], the role of the chemical character of the dopant – oxygen bonds were found determinative for the hydroxyde ion stabilization as well as for the O-H bond strengths deduced from the computed O−H stretching frequencies. Whereas the formation of protonic defects leads to a higher stabilization of Y-doped zirconates, the O-H stretching in these oxides is red-shifted by 250 − 1500 cm^{-1} in comparison to the same structural configurations in In- and Sc- doped $BaZrO_3$.

2. Models and Computational details

Models of M-doped $BaZrO_3$ consist of three different 2x2x2 supercells with 12.5 (BZM12.5), 25 (BZM25) and 37.5% (BZM37.5) dopant concentrations with M = Sc and In, where one, two or three Zr^{4+} ions were replaced by the M^{3+} ions, respectively. The charge neutrality is respected by inserting one, two and three H-ions, respectively, in BZM12.5, BZM25 and BZM37.5 models. The compositions of the studied supercells are $Ba_8Zr_7MHO_{24}$ (BZHM12.5), $Ba_8Zr_6M_2H_2O_{24}$ (BZHM25) and $Ba_8Zr_5M_3H_3O_{24}$ (BZHM37.5). In addition, two possible supercells were considered for two different dopant positions in the BZM25 and BZM37.5 models, leading to two minimum energy structures. The most stable structures for both 25 and 37.5 % dopant concentrations are those with M−O−M dopant configurations as shown in Figure 1 (left side). Consideration of the three possible oxygen sites, labeled in Figure 1 as O1 (Zr−O−Zr), O2 (M−O−Zr) and O3 (M−O−M), allowed examining also the effect of dopant arrangements in the oxide network on the stabilization of hydroxide ions into the host-oxide.

Computations based on the periodic Density Functional Theory were carried out with Crystal09 computer program [37]. For the exchange-correlation (XC) functional the hybrid B3LYP approximation [38, 39] was used. The atomic orbitals were described with Gaussian basis sets as follows: effective core-potentials (ECP) used for Ba – HAY&WADT-Small core

ECP [40] and In – DURAND-21d1G [41]; all electron basis sets for Zr [42], Sc [43], Y, [44], O (8-411d11G) [45] and H (H_3-1p1G) [46]. Those input parameters have been chosen based on our benchmark calculations for crystal cell constant, electronic band gap and vibrational frequencies of the ideal $BaZrO_3$ cubic crystal [29] and their comparison with the respective experimental results [47-49].

Computational tolerances for controlling the accuracy of Coulomb and exchange, and correlation series were set equal to: 10^{-7}, 10^{-7}, 10^{-7}, 10^{-7} and 10^{-24}. A shrinking factor of 4 x 4 was used to generate the commensurate k-points grid in the reciprocal space within the Pack-Monkhorst method [50]. Atomic positions and crystal cells were fully optimised by employing the analytical geometry optimization based on a quasi-Newton optimization scheme with Broyden-Fletcher-Goldfarb-Shano (BFGS) algorithm for the Hessian matrix updates using the corresponding implementations in the Crystal program [37]. The vibrational spectra were computed at Γ-point in the harmonic approximation for the optimized crystal structures. Details on the implementation of vibrational frequency computations in Crystal code can be found elsewhere [51].

3. Results and Discussion

3.1 Structural properties of $BaZr_{1-x}M_xH_xO_3$ (M = In and Sc; x=0.125; 0.25 and 0.375)

The oxide structural deformations induced by hydrogen insertion are first analyzed for the 12.5% doped $BaZrO_3$. The formation of hydroxide ions at O1 and O2 sites, drawn in Scheme 1, led to a Pm symmetry, pointing to a strong symmetry reduction in comparison to the cubic (Fm3m) cells of the hydrogen-free $BaZr_{0.875}M_{0.125}$ models with a computed cell constant of 4.247 Å and 4.248 Å for In and Sc dopant, respectively. The computed structural details for $BaZr_{0.875}M_{0.125}H_{0.125}O_3$ (M=In and Sc) are collected in Table 1. In the H-containing structures, one of the cell constant elongates slightly by ~0.5% whereas the other two slightly shrink. As a result, there is a nearly negligible volume expansion of the crystals with a hydroxide ion.

An elongation of the M−O/Zr−O distances is obtained only in the octahedrons with O−H bonds due to the displacements of the two oxygens involved in the hydrogen bonds as illustrated in Scheme 1. In general, the computed interatomic distances in BZHI12.5 agree well with those measured with EXAFS for hydrated BZI samples with In concentrations ranging from 75% down to 2% , being shorter by only 0.01 – 0.02 Å in the dry samples with acceptor-dopant percentages ≥ 10% [10]. Two Zr–Ba distance sets in both BZI and BZS systems have been evidenced from the EXAFS analysis [10] in good agreement with the present

computational results, giving one short and one long Zr−Ba distances with the averaged values of ~3.6 Å and of ~3.82 Å, respectively. Considering the M–Ba distances, an increased local distortion is found only if a hydrogen is bound to O2 ion in Zr−O−M configuration. This is also consistent with the EXAFS results [10], reporting two distance shells for In–Ba of 3.59 and 3.74 - 3.76 Å. Our results showed systematically a somewhat stronger structural deformation in the H-containing regions than those obtained from the EXAFS analysis. This could be related to the possible coexistence of other than hydroxide defects in the as synthesized samples. In addition, the H-bonds formed in structures **1a** and **1b** are not linear. The O2(O1)−H…O2 angle amount to 137.9 (131.1˚) and the OH…O distances are 2.004 Å (**1a**) and 2.050 Å (**1b**). Very similar structural properties were obtained in 12.5% Y-doped $BaZrO_3$ with hydroxide ions [29].

In the structures with two and three acceptor-dopants, corresponding to BZHM25 and BZHM37.5, the effect of hydrogen mutual orientations and the distance between the hydroxide defects has been examined. As shown in Scheme 2, two possible hydrogen orientations were considered for the parallel, *p*, and anti-parallel, *a*, mutual O−H bonds. Hydroxide ion formations at O1, O2 or O3 sites have been examined by exploring a large number of possible combinations between them. The symmetries of the cells are again reduced to P1 or P2 space groups, similarly to our previous results for $BaZr_{1-x}Y_xH_xO_3$ (x = 0.25 and 0.375). The structural parameters closely resemble those in the 12.5% In and Sc doped $BaZrO_3$ (Table 1). An important difference with the Y dopant is that hydroxide defect formations in Y−OH−Y configurations were not established, whereas In-OH-In and Sc-OH-Sc configurations led to energetically stable crystal structures. Moreover, the strong structural distortion established for the BZHY37.5 models [29] due to the increased $Y^{3+}…Y^{3+}$ attraction in the H-containing octahedrons, were not been obtained either for In or for Sc dopant. These results are in line with most of the recent experimental evidences concluding to a nearly same dopant solubility, hydration rate, proton conductivity and itneratomic distances for In- doped barium zirconates [3, 10] as well as to high similarities between BZI and BZS oxides [3, 7].

In most of the minimum energy structures non-linear hydrogen bonds with an O–H…O angle in the range of 100 to 140˚ were formed. Linear H-bonds (with 178˚) are found only in BZHI25 and BZHS25 with anti-parallel O1–H hydroxides in the same octahedron with two OH…O bond lengths in the interval of 2.3–2.6 Å. In the structures with at least one O2–H hydroxide there is systematically only one short hydrogen bond with 1.91–1.98 Å length. The O3–H…O1/O2 hydrogen bonds are slightly longer (2.1–2.2 Å).

In overall, the optimized geometrical parameters in In-, Sc- and Y-doped structures reveal a high similarity. It is thus not possible to discriminate between Y, In and Sc dopants considering only the structural deformations, induced by the three dopants.

Further on, the atomic charges, computed following Mulliken population scheme [52], do not vary significantly (within an accuracy of 0.02 e^-) with In and Sc dopant, their concentration and distribution in the supercell. The charges at Zr, q(Zr) and at Ba, q(Ba), sites are 2.9 and 1.8 e, respectively, and the charge at H is between 0.3 – 0.4 e^- in all the considered structures. For both In and Sc ions $q \approx 2\ e^-$ was obtained. This value is higher than the charge at Y site(s) in BZY found in the range of 0.6 - 1 e^- and depending on the Y amount in the barium zirconate [29]. The next important difference between the zirconates with Y and with In/Sc dopants are the oxygen charges. Whereas q(O) in the three Zr–O1–Zr, Zr–O2–M and M–O3–M configurations in all BZHI and BZHS structures equals to ~ -1.5 – -1.6 e^-, a notable variation between the oxygen charges in BZHY has been established as a function of oxygen nearest environment, following the trend q(O1) > q(O2) > q(O3) [29]. This charge variation was related to the clear evidences of the strong covalent (with an antibonding character) Y−O bond. Similar bond order analysis, using the Overlap Population (OP) matrix elements, revealed that Sc interacts only electrostatically with the neighbor oxygen, because zero OP matrix elements for Sc–O bonds were computed. In–O bond is also rather ionic with a partial covalent contribution of a maximum of 13% with a bonding character, thus indicating a predominantly ionic In-O bond type. The similarity of the oxygen charges in those models is thus associated with the ionic In/Sc−O bond type, which is the same as the Zr-O ionic bonds.

Because the type of M−O chemical bond is expected to affect the electron density at an oxygen site, which is related with its capability to participate in the hydroxide ion formations, the M-O bond character seems to be in the origin of the observed proton conduction differences between BZY and BZI (BZS). The well established covalent Y–O bond leads to strong electron density redistribution in the near dopant region, indicating an oxygen basicity decrease, which is mostly pronounced in the Y−O−Y configurations. In the case of In or Sc ions the formation of ionic bonds with the oxygen ions, does not modify q(O), which remains same as in the undoped BZ structures. The very comparable proton transferability observed experimentally for In/Sc dopant can be first related to the similar capability of the three possible oxygen centers to form hydroxides in a large range of dopant concentrations. In the contrary, the increased Y-concentration or segregation of Y defects offering a higher number of Y–O–Y configurations is not expected to allow a high concentration of protonic defects, because O3 sites are very unlikely to accommodate hydroxide ions [29].

3.2 Hydrogen insertion energies

The H insertion energies in the minimum energy states with protonic defects have been computed from the equation $\Delta E(H) = 1/n\ [E(BZHM) - E(BZM) - n.E(H)]$, where n is the number of hydrogens. Comparable H binding energies in In- and Sc-doped $BaZrO_3$ for the same local environment(s) were calculated as is evidenced from the $\Delta E(H)$ values in Figure 2. The strongest H-oxide interaction is found for the hydroxide ion formed at O2 site, equal to -2.35 eV in BZHS12.5 and to -2.38 eV in BZHI12.5. Hydrogen binding to O1 stabilizes less the host oxide, by 0.4 eV. The H-binding to O2 sites remains more favored also in the models with 25% dopants, although the difference with the hydrogen insertion energy at O1 sites becomes smaller. This effect is more pronounced for the Sc than for In acceptor-dopant. Taking for instance the difference, $\Delta(\Delta E(H))$, between the most stable structures containing hydroxides in O1H–O1H-a and in O2H–O2H-a configurations, we obtained $\Delta(\Delta E(H)) = 0.32$ eV in the case of BZHS25 and 0.07 eV in BZHI25. The H binding energy increases even more if at least one of the hydrogen binds to an O3 site. A very slight stabilization due to the hydrogen insertion is observed with the increase of the acceptor dopants up to 37.5% in both doped oxides. Again, this trend is somewhat more pronounced for Sc than for In-dopant.

The mutual hydrogen orientations influence the H binding if the two or three O−H bonds are in the same octahedron, separated by a distance of about 4 Å. Anti-parallel displacements between the two hydrogens bound to two neighbor anions in the 25% of dopants led always to more stable structures, than those with parallel O−H bond orientations. This shows that in the latter case, the repulsion between the hydrogens is stronger and hence decreases the O-H interaction. Same effect has been observed for the H binding strength in Y-doped $BaZrO_3$ and as expected this effect becomes unimportant for O−H separations by more than one cation in the host oxide. Interestingly, theoretical investigation with DFT-GGA approximation reported on attractive hydroxide interactions of parallel and closely spaced OH defects in undoped $SrTiO_3$ [53]. This difference can be ascribed on the interplay between linear and short (strong) hydrogen bonds that stabilize the oxide network, and the repulsion between two closely lying positively charged ends of the two OH species. Indeed, two linear and short H-bonds were obtained in doped $BaZrO_3$ with two anti-parallel OH defects in the same octahedron (see section 3.1).

Hydrogen interaction energies with the BZY oxides [29] with the same O−H binding configurations as in BZHI(S) are systematically stronger by 0.3 – 0.5 eV if at least one O2 cite

is involved in the hydroxide ion formation and by 0.2 – 0.6 eV in the structures with only O1−H hydroxides.

3.3 Lattice dynamics

The lattice dynamics of $BaZr_{1-x}M_xO_3$ (M = Y, In and Sc, and x = 0.125, 0.25) has been investigated trough the computed vibrational spectra for the optimized minimum energy structures. In all cases, the Hessian matrix has only positive eigenvalues, e.g. only positive vibrational frequencies are obtained, which confirms that the structures are ground states on the potential energy surface. The characteristic fingerprint of protonic defects in the vibrational spectrum of hydrated perovskite is the O−H stretching band usually located in the 2500 – 3500 cm^{-1}. The host oxide vibrations are bellow 1000 cm^{-1} and their deviation from the vibrational structure in the ideal cubic barium zirconate indicates local structural distortions [7,8].

In Tables 2 and 3, the computed oxide-lattice vibrations and O−H stretching and bending modes, respectively, are collected. Due to the symmetry distortion, there is a splitting of the three characteristic bands, identified in the ideal $BaZrO_3$: Zr(M)–O stretching, O–Zr(M)–O bending and Ba-ZrO_6 stretching. Studies with Infra Red (IR) and Raman spectroscopies applied to $BaM_{0.10}Zr_{0.90}O_{2.95}$ (M=Y, In, Sc and Ga) [7] and to $BaIn_xZr_{1-x}O_{3-x/2}$ (x=0, 0.10, 0.25, 0.375, 0.50, 0.625 and 0.75) [8] reported on the deviation from cubic symmetries. The computed by us Zr(M)–O stretching in the interval of ~450 – 800 cm^{-1}, O–Zr(M)–O bending in the region of ~250 – 550 cm^{-1} and Ba-ZrO_6 stretching between 60 – 150 cm^{-1} are in very good agreement with the experimental data [7,8]. The mode at 620 – 650 cm^{-1} assigned from the computations to Zr(M)–O stretching vibration corresponds to the experimentally observed shoulder at around 600 cm^{-1} [7]. The host-oxide vibrations are only slightly affected by the dopant nature, confirming the structural similarities as discussed in Section 3.1. Analogous conclusions were drawn from the experimental spectra in the range below 1000 cm^{-1}, found to exhibit nearly identical vibrational features in the studied doped barium zirconates [7].

The O−H stretching and bending modes vary however with local OH environment and they are significantly influenced by the dopant. Moreover, the theoretical vibrational analysis allows distinguishing precisely between various OH sites, dopant ion and their concentration into the host oxide. The O-H stretching modes in several doped zirconates and cerates were reported to undergo a red shift compared to the stretching vibration of the isolated OH^-, ν_{OH^-} =

3556 cm^{-1} [54]. A red shift was detected in most of the good proton conducting oxides indicating a softening of the fundamental vibrational mode [54].

The present calculations yielded a red shift of the O-H stretching band(s), reported in Table 3, in the majority of the considered structures. The computed with same numerical details ν_{OH}^- is 3623 cm^{-1}. The O−H shift to the lower frequencies is mostly pronounced in the BZHY structures with O2−H hydroxide(s), indicating a weaker O2−H bond than in the BZHI(S) oxides, despite the obtained better stabilization of the Y-doped zirconates by the hydrogen insertion in comparison to In and Sc doped ones (see Section 3.2). The O1−H stretching bands in all oxides with 12.5% doping concentration fall in the range of 1510 – 1610 cm^{-1} remaining close to the ν_{OH}^- in gas-phase, and alike to the O2−H stretching in In and Sc doped zirconates. The computed stretching frequencies correlate well with the variation of the O−H bond lengths: O2−H bonds are longer by ~0.01 Å than O1−H in BZHY12.5 [29], whereas they are very comparable to O1−H in BZHI(S)12.5 structures (Table 1). Moreover, the covalent Y−O bond and the associated decrease of electron density at O2 site in BZY are indeed expected not to form strong O2−H bonds.

The tendency of decreasing the O2−H stretching in Y-doped $BaZrO_3$ by ~250 - 300 cm^{-1} is well preserved also at a higher doping content as follows from the values in Table 3 for $BaY_{0.25}Zr_{0.75}H_2O_3$. For the three dopant ions the dopant uptake does not play an important role on the O−H stretching for a particular oxygen environment, except in the structures with anti-parallel O−H mutual orientations (structures **O1-O1-a** and **O2-O2-a** in Table 3). The red shift computed in these structures is mostly evidenced for Y-dopant: the O−H stretching is at 2100 cm^{-1} in structure **O1-O1-a**. There is also an important decrease of the frequencies (~250 cm^{-1}) in BZI and BZS with two anti-parallel O-H bonds. This can be explained with the formation of short and linear H-bonds (with 178˚) as discussed in the Section 3.1, which is expected to decrease the O−H strength. A direct linear correlation between the shortening of the hydrogen bond lengths in $Ba_2In_2O_4(OH)_2$ and the decrease of the O-H stretching frequency values has been established in ref. 34 from the DFT computational analysis. It was also found that when the OH stretching softens the in-plane and out-of-plane OH bending stiffen [34]. Same tendency is evidenced from our results in Table 3. If the two O1−H bonds are parallel, the oxide networks are less stable compared to the anti-parallel O−H bond displacements, but the O−H force increases.

In average, the O−H stretching bands lies at lower frequencies in the Y-doped structures than those in the In or Sc doped ones. This point to the conclusion, that Y-dopant does not cause a strong trapping of hydrogen in the host oxide as compared to the stronger

O−H bonds in most of the possible H-containing models of In and Sc-doped barium zirconates. On the other side, the formation of hydroxide ions, especially at O2 sites favor the host-oxide stabilization (Figure 2) and this tendency is more pronounced for Y-dopant.

The O-H in plane bending frequency is surprisingly high in $BaY_xZr_{1-x}H_xO_3$ (x=0.125 and 0.25). It suggests a stronger interaction between hydrogen and the neighbor ions, most probably due to the elongated O2−H bond. Experimentally, vibrational features in the 1500 – 2500 cm^{-1} region have been observed as well, assigned however to the O−H stretching [54]. The frequency assignment in our theoretical study is straightforward from the normal vector analysis.

4. Conclusion

Local and long range structural properties of In- and Sc-doped $BaZrO_3$ (2x2x2) supercell models with increase of the dopant content from 12.5, to 25, to 37.5% were studied in a systematic way. The results showed very similar geometrical and electronic properties for both dopants and various concentrations. Only ionic Sc – O bonds were formed. In–O bonds have also a predominant ionic character with a small covalent (bonding) contribution up to 13% maximum. This is the only important difference with respect to the results obtained for the Y-dopants [29], forming predominantly covalent Y-O bonds with an anti-bonding character.

Energetically favored formation of hydroxide ions is established at the O1, O2 and O3 oxygen centers in BZHI and BZHS at variance from Y-doped $BaZrO_3$, where an O3−H protonic defect was not obtained. The latter result is associated with the pronounced decrease of the oxygen electronic charge, indicating a smaller basicity in Y−O3−Y in comparison to the O2 and O1 centers. Hydroxide ion formation is generally favored for the near dopant oxygens, independent on the chemical nature of the studied acceptor-dopant ions. The long range arrangements have an almost negligible impact on the hydroxide ion formations and near dopant structural and electronic properties.

The oxide-lattice dynamics, studied from the computed vibrational frequencies of $BaM_xZr_{1-x}H_xO_3$ (M=In, Sc and Y; x=0.125 and 0.25), is not affected by the dopant chemical nature. However, the dopant-oxygen bond character and the formation of linear hydrogen bonds have been evidenced as the most important factors leading to red shifts ranging from ~300 to ~1500 cm^{-1} of the O−H stretching vibrations, thus indicating an important decrease of the O−H bond strengths. Nevertheless the largest oxide stabilization due to hydrogen insertion is found for Y-dopant, the O−H stretching modes in BZHY are generally red-shifted compared

to those in BZHI and BZHS. This shows weaker O−H bonds in Y-doped structures than in In and Sc doped barium zirconates.

Acknowledgments: This work was supported by the European Union (EU-NMP-India-CP-FP 233482 HYPOMAP). Part of the calculations was performed at the HPC resources under the allocation x2013086396 made by GENCI (Grand Equipement National de Calcul Intensif).

References:

[1] K.D. Kreuer, St. Adams, W. Munch, A. Fuchs, U. Klock, J. Maier, Solid State Ionics 145 (2001) 295–306.

[2] K.D. Kreuer, Solid State Ionics 97 (1997) 1-15.

[3] S. Imashuku,T. Uda, Y. Nose, G. Taniguchi, Y. Ito, Y. Awakura**,** J. Electrochem. Soc. 156 (2009) B1 – B8.

[4] F. Giannici, A. Longo, K.D. Kreuer, A. Balerna, A. Martorana, Solid State Ionics 181 (2010) 122 – 125.

[5] F. Giannici, A. Longo, A. Balerna, K. D. Kreuer, A. Martorana, Chem. Mater. 19 (2007) 5714 – 5720.

[6] T. Norby, M. Widerøe, R. Glöckner, Y. Larring, Dalton Trans. (2004) 3012-3018.

[7] M. Karlsson, I. Ahmed, A. Matic, S. G. Eriksson, Solid State Ionics 181 (2010) 126 – 129.

[8] M. Karlsson, A. Matic, C. S. Knee, I. Ahmed, S. G. Eriksson, L. Börjesson, Chem. Mater. 20 (2008) 3480 – 3486.

[9] M. Karlsson, A. Matic, S. F. Parker, I. Ahmed, L. Börjesson, S. Eriksson, Phys. Rev. B 77 (2008) 104302 – 106308.

[10] F. Giannici, A. Longo, A. Balerna, K.D. Kreuer, A. Martorana, Chem Mater. 21 (2009) 2641– 2649.

[11] F. Giannici, M. Shirpour, A. Longo, A. Martorana, R. Merkle, J. Maier, Chem. Mater. 23 (2011) 2994 – 3002.

[12] K.D. Kreuer, Annu. Rev. Mater. Res. 33 (2003) 333 – 359.

[13] T. Schober, H.G. Bohn, Solid State Ionics 127 (2000) 351 – 360.

[14] H. G. Bohn, T. Schober, J. Am. Ceram. Soc. 83 (2000) 768 – 772.

[15] Y. Yamazaki, P. Babilo, S. M. Haile, Chem. Mater. 20 (2008) 6352 – 6357.

[16] A. K. Azad, Ch. Savaniu, S. Tao, S. Duval, P. Holtappels, R. M. Ibberson and J. T. S. Irvine, J. Mater. Chem. 18 (2008) 3414 – 3418.
[17] U. Anselmi-Tamburini, M. T. Buscaglia, M. Viviani, M. Bassoli, C. Bottino, V. Bascaglia, P. Nanni, Z. A. Munir, J. Eur. Ceramic. Soc. 26 (2006) 2313 – 2318.
[18] P. A. Stuart, T. Unno, R. Ayres-Rocha, E. Djurado, S. J. Skinner J. Eur. Cer. Soc. 29 (2009) 697 – 702.
[19] F. Iguchi, T. Tsurui, N. Sata, Y. Nagao, H. Yugami, Solid State Ionics 180 (2009) 563–568.
[20] F. Iguchi, N. Sata and H. Yugami, J. Mater. Chem. 20 (2010) 6265–6270.
[21] R. B. Cervera, Y. Oyama, S. Miyoshi, K. Kobayashi, T. Yagi, S. Yamaguchi, Solid State Ionics 179 (2008) 236 – 242.
[22] S. B. C. Duval, P. Holtappels, U. F. Vogt, U. Stimming, T. Graule, Fuel Cells 9 (2009) 613–621.
[23] M. E. Björketun, P. G. Sundell, and G. Wahnström, Phys. Rev. B 76 (2007) 054307 – 054316.
[24] M. A. Gomez, M. Chunduru, L. Chigweshe, L. Foster, S. J. Fensin, K. M. Fletcher, L. E. Fernandez, J. Chem. Phys. 132 (2010) 214709-1– 8.
[25] B. Merinov, W. Goddard III, J. Chem. Phys. 130 (2009) 194707-1– 6.
[26] A. V. Bandura, R. A. Evarestov, D.D. Kuruch, Surf. Sci 604 (2010) 1591 – 1597.
[27] R. A. Evarestov, A. V. Bandura, Solid State Ionics, 188 (2011) 25-30.
[28] D.-H. Kim, B.-K. Kim, Y.-C. Kim, Solid State Ionics 213 (2012) 18–21.
[29] D. Zeudmi Sahraoui, T. Mineva, Solid State Ionics, 232 (2013) 1–12.
[30] P. Berastegui, S. Hull, F. J. Garcia-Garcia, S.-G. Eriksson, J. Solid State Chem. 164 (2002) 119–130.
[31] I. Ahmed, C. S. Knee, M. Karlsson, S.-G. Eriksson, P. F. Henry, A. Matic, D. Engberg, L. Börjesson, J. Alloys Comp. 450 (2008) 103-110.
[32] S. Stølen, C. E. Mohn, P. Ravindran, N. L. Allan, J. Phys. Chem. B 109 (2005) 12362-12365.
[33] S. Stølen, E. Bakken, C. E. Mohn, Phys. Chem. Chem. Phys. 8 (2006) 429-447.
[34] J.-R. Martinez, C. E. Mohn, S. Stølen, N. L. Allan, J. Solid State Chem. 180 (2007) 3388–3392.
[35] I. Ahmed, M. Karlsson, S.-G. Eriksson, E. Ahlberg, C. S. Knee, K. Larsson, A. K. Azad, A. Matic, L. Börjesson, J. Am. Ceram. Soc., 91 (2008) 3039-3044.

[36] I. Oikawa, M. Ando, Y. Noda, K. Amezawa, H. Kiyono, T. Shimizu, M. Tansho, H. Maekawa, Solid State Ionics 192 (2011) 83-87.
[37] V. R. Saunders, R. Dovesi, C. Roetti, R. Orlando, C. M. Zicovich-Wilson, F. N. M. Pascale, B. Civalleri, K. Doll, N. M. Harrison, I. J. Bush, P. D'Arco, M. Llunell, *CRYSTAL 09 user's manual*; Universita' degli Studi di Torino: Torino, Italy, 2008.
[38] A. D. Becke, J. Chem. Phys. 98 (1993**)** 5648 – 5652.
[39] C. Lee, W. Yang, R. G. Parr, Phys. ReV. B 37 (1988) 785 – 789.
[40] S. Piskunov, E. Heifets, R.I. Eglitis, G. Borstel, Comp. Mat. Science 29 (2004) 165 – 178.
[41] M. Causa, R. Dovesi, C. Roetti, Phys. Rev. B. 43 (1991) 11937– 11943.
[42] http://www.crystal.unito.it/Basis_Sets/zirconium.html
[43] http://www.crystal.unito.it/Basis_Sets/scandium.html
[44] A. Buljan, P. Alemany, E. Ruiz, J. Phys. Chem. B 103 (1999) 8060**–**8066.
[45] L. Valenzano, F.J. Torres, K. Doll, F. Pascale, C.M. Zicovich-Wilson, R. Dovesi, Z. Phys. Chem. 220 (2006) 893 – 912.
[46] C. Gatti, V.R. Saunders, C. Roetti, J. Chem. Phys. 101 (1994) 10686 – 10696.
[47] W. Pies and A. Weiss, in *Landolt-Börnstein: Numerical Data and Functional Relationships in Science and Technology*, edited by K.-H. Hellweg and A. M. Hellwege, New Series, Group III, Vols. 7b1 Springer, Berlin, 1975 and 7e Springer, Berlin, 1975.
[48] J. Robertson, J. of Vac. Sci. Technol. B 18 (2000) 1785-1791.
[49] C.H. Perry, D.J. Mccarthy, G. Rupprech, Phys. Rev. 138 (1965) A1537-A1538.
[50] H. J. Monkhorst and J.D. Pack, Phys. Rev. 13 (1976) 5188 – 5192.
[51] F. Pascale, C. M. Zicovich-Wilson, F. Lopez, B. Civalleri, R. Orlando, R. Dovesi J. Comput. Chem. 25 (2004) 888-897.
[52] R. S. Mulliken, 23 (1955) 1833–1840.
[53] N. Bork, N. Bonanos, J. Rossmeisl and T. Vegge, Phys. Chem. Chem. Phys., 13 (2011) 15256–15263.
[54] K. D. Kreuer, Solid State Ionics 125 (1999) 285-302.

Table 1. Averaged interatomic distances and cell parameters in **Å** in BZHI12.5 and BZHS12.5 systems. O1 (Zr-O-Zr) and O2 (Zr-O-M) hydrogen binding sites of optimised models are indicated.

Dopant, M	Binding site	M-O	Zr-O	M-Ba	Zr-Ba	Ba-O(H)	O-H	Cell constants[a)]
In	O2	2.126 ± 0.07(x5) 2.238	2.134 ± 0.03 2.298	3.605 3.825	3.653 ± 0.04 (x5) 3.771 ± 0.05 (x2)	3.184	0.971	a = 4.238 b = 4.253 c = 4.270
	O1	2.155 (x3) 2.188 (x3)	2.130 ± 0.04 (x19) 2.258 ± 0.01 (x2)	3.639	3.651 ± 0.08 (x5) 3.877 ± 0.01 (x2)	3.189	0.974	a = 4.242 b = 4.270 c = 4.257
Sc	O2	2.040 2.144 ± 0.04 (x4) 2.255	2.135 ± 0.02 (x20) 2.279 (x1)	3.606 3.823	3.654 ± 0.04 (x6) 3.770 ± 0.04 (x2)	3.181	0.972	a = 4.242 b = 4.271 c = 4.259
	O1	2.146 (x2) 2.153 (x2) 2.186 (x2)	2.132 ± 0.03 (x19) 2.259 ± 0.01 (x2)	3.638	3.672 ± 0.05 (x4) 3.876 ± 0.01 (x2) 4.046	3.187	0.974	a = 4.242 b = 4.271 c = 4.259

[a)]The cell constants in the hydrogen-free $BaZr_{0.875}M_{0.125}$ models with Fm3m symmetry, obtained with the same theoretical method (see text), are 4.247 and 4.248 Å for In^{3+} and Sc^{3+} dopant, respectively.

Table 2. Oxide lattice vibrational frequencies in cm^{-1} in $BaM_xZr_{1-x}H_xO_3$ (x =0.125 and 0.25, M=Y, Sc and In).

Assignment	Y	Sc	In
Zr(M) – O stretching	821 – 456	799 – 453	798 - 450
O - Zr(M) –O	450 - 270	449 - 243	437 - 260
ZrO_6 torsional motion	233 - 169	238 - 191	244 - 184
Ba-ZrO_6	139 – 60	156 - 81	150 - 73

Table 3. Vibrational frequencies in cm^{-1} in $BaZr_{1-x}M_xH_xO_3$ (x=0.125 and 0.25; M=Y, Sc and In). For comparison the computed with same numerical details stretching vibration in gas-phase OH^-, ν_{OH^-}, is 3623 cm^{-1}.

Structure	H-binding site	O-H stretching	O-H bending in plane	O-H bending out of plane
$BaY_{0.125}Zr_{0.875}HO_3$	O1	3510	1003	957
	O2	3389	1711	837
$BaSc_{0.125}Zr_{0.875}HO_3$	O1	3542	1047	1030
	O2	3576	961	915
$BaIn_{0.125}Zr_{0.875}HO_3$	O1	3562	1040	926
	O2	3607	941	879
$BaY_{0.25}Zr_{0.75}H_2O_3$	O1-O1-a	2091; 2128	1727; 1728	1145; 1151
	O1-O1-p	3534; 3657	1020; 1020	843; 899
	O1-O2-a	3393; 3659	1898; 1563	1564; 1017
	O2-O2-a	3339; 3344	1734; 1683	1513; 1231
$BaSc_{0.25}Zr_{0.75}H_2O_3$	O1-O1-a	3391; 3397	1288; 1287	874; 869
	O1-O1-p	3753; 3755	905; 902	820; 787
	O1-O3-a	3726; 3785	968; 880	818; 813
	O2-O2-a	3486; 3486	1040; 1042	911; 917
$BaIn_{0.25}Zr_{0.75}H_2O_3$	O1-O1-a	3415; 3420	1281; 1279	879; 874
	O1-O1-p	3747; 3748	895; 897	790; 895
	O1-O3-a	3751; 3799	1002; 897	867; 844
	O2-O2-a	3469; 3499	1064; 1054	943; 938

Captions for Figures

Figure 1. $BaZr_{0.75}M_{0.25}O_3$ (left) and $BaZr_{0.625}M_{0.375}O_3$ (right) (M^{3+} = Sc^{3+} and In^{3+}) energetically most stable structures with oxygen anions in three different local environments: Zr−O1−Zr, Zr−O2−M and M−O3−M configurations.

Scheme 1. Schematic presentation of the two ground state structures of BZHM12.5 (M = Sc^{3+} and In^{3+}) with hydrogen bound to O2 (*1a*) and O1(*1b*).

Scheme 2. Schematic presentation of hydrogen displacements considered in BZM25 and BZM37 structures. Anti-parallel (a) and parallel (p) O-H mutual orientations are illustrated in structures O1-O1-a, O1-O1-p, respectively. Analogous configurations were considered for hydrogen binding to O2 and O3 sites and to combinations of them.

Figure 2. Hydrogen binding energy as a function of oxygen binding sites in BZHS (top) and BZHI (bottom) for dopant concentrations of 12.5 (one OH in the supercell), 25 (two OH in the supercell) and 37.5% (three OH in the supercell). For the labeling of the mutual hydrogen displacements see Scheme 2.

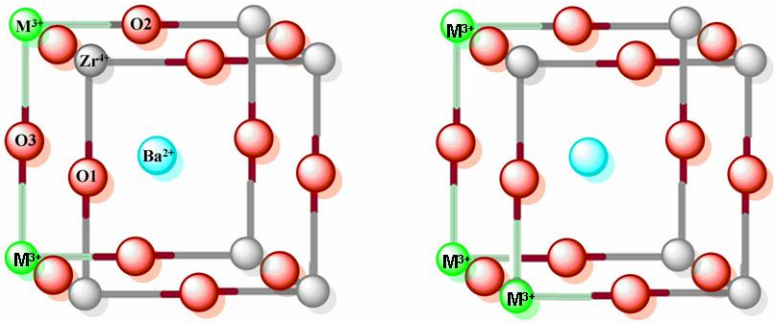

Figure 1. $BaZr_{0.75}M_{0.25}O_3$ (left) and $BaZr_{0.625}M_{0.375}O_3$ (right) (M = Sc^{3+} and In^{3+}) energetically most stable structures with oxygen anions in three different local environments: Zr−O1−Zr, Zr−O2−M and M−O3−M configurations.

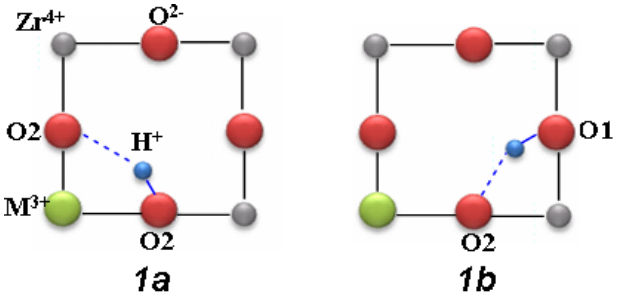

Scheme 1. Schematic presentation of the two ground state structures of BZHM12.5 (M = Sc^{3+} and In^{3+}) with hydrogen bound to O2 (*1a*) and O1(*1b*).

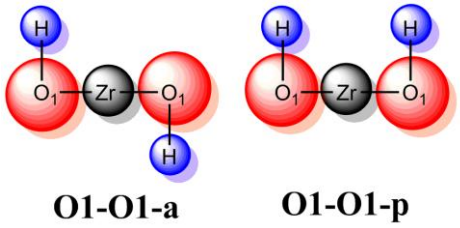

Scheme 2. Schematic presentation of hydrogen displacements considered in BZM25 and BZM37 structures. Antiparallel (a) and parallel (p) O-H mutual orientations are illustrated in structures O1-O1-a, O1-O1-p, respectively. Analogous configurations were considered for hydrogen binding to O2 and O3 sites and to combinations of the three different oxygen centers.

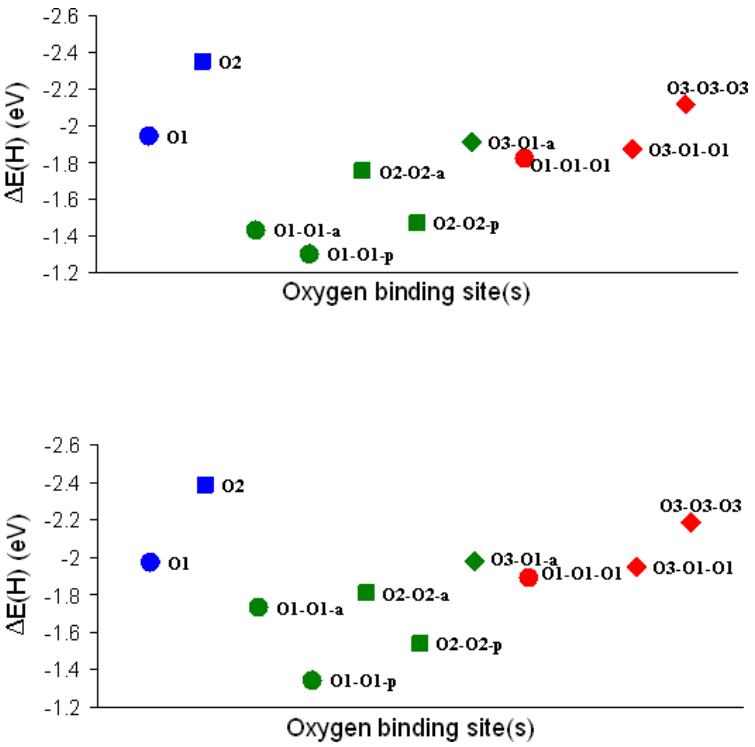

Figure 2. Hydorgen binding energy as a function of O1, O2 and O3 binding sites in BZHS (top) and BZHI (bottom) for dopent concentrations of 12.5 (one OH in the supercell), 25 (two OH in the supercell) and 37.5% (three OH in the supercell). For the labeling of the mutual hydrogen displacements see Scheme 2.

Table of Contents Graphic